PAPER

Understanding the defect chemistry of alkali metal strontium silicate solid solutions: insights from experiment and theory†

Ryan D. Bayliss,[*ab] Stuart N. Cook,[c] David O. Scanlon,[de] Sarah Fearn,[b] Jordi Cabana,[a] Colin Greaves,[f] John A. Kilner[bg] and Stephen J. Skinner[b]

Recent reports of remarkably high oxide ion conduction in a new family of strontium silicates have been challenged. It has recently been demonstrated that, in the nominally potassium substituted strontium germanium silicate material, the dominant charge carrier was not the oxygen ion, and furthermore that the material was not single phase (R. D. Bayliss *et. al.*, *Energy Environ. Sci.*, 2014, DOI: 10.1039/c4ee00734d). In this work we re-investigate the sodium-doped strontium silicate material that was reported to exhibit the highest oxide ion conductivity in the solid solution, nominally $Sr_{0.55}Na_{0.45}SiO_{2.775}$. The results show lower levels of total conductivity than previously reported and sub-micron elemental mapping demonstrates, in a similar manner to that reported for the $Sr_{0.8}K_{0.2}Si_{0.5}Ge_{0.5}O_{2.9}$ composition, an inhomogeneous chemical distribution correlating with a multiphase material. It is also shown that the conductivity is not related to protonic mobility. A density functional theory computational approach provides a theoretical justification for these new results, related to the high energetic costs associated with oxygen vacancy formation.

Introduction

Singh and Goodenough recently reported rapid oxide ion conductivity[2,3] in several compositions of monoclinic $Sr_{1-x}A_x$-$MO_{3-0.5x}$ (A = Na, K; M = Si and/or Ge). The crystal chemistry was subsequently investigated with *in situ* high temperature neutron diffraction by Martinez *et al.*[4] and the nominal $Sr_{0.55}$-$Na_{0.45}SiO_{2.775}$ composition has been shown to operate surprisingly well in application as a fuel cell electrolyte by Wei *et al.*[5] A solid state nuclear magnetic resonance study has also recently been published focusing on the Si local environment.[6] These newly proposed electrolyte materials have been reported to possess oxide ion conductivities as high as 1.79×10^{-2} S cm^{-1}

[a]*Department of Chemistry, University of Illinois at Chicago, 845 W. Taylor Street, Chicago, Illinois, 60607, USA. E-mail: rbayliss@uic.edu*

[b]*Department of Materials, Imperial College London, Prince Consort Road, London SW7 2BP, UK*

[c]*Department of Materials Science and Engineering, Massachusetts Institute of Technology, Cambridge, Massachusetts 02139-4307, USA*

[d]*University College London, Kathleen Lonsdale Materials Chemistry, Department of Chemistry, 20 Gordon Street, London WC1H 0AJ, UK*

[e]*Diamond Light Source Ltd., Diamond House, Harwell Science and Innovation Campus, Didcot, Oxfordshire OX11 0DE, UK*

[f]*School of Chemistry, University of Birmingham, Birmingham B15 2TT, UK*

[g]*International Institute for Carbon-Neutral Energy Research (I2CNER), Kyushu University, 744 Motooka, Nishi-ku, Fukuoka, 819-0395, Japan*

† Electronic supplementary information (ESI) available. See DOI: 10.1039/c4ta04299a

at 550 °C in the $Sr_{0.55}Na_{0.45}SiO_{2.775}$ material with a remarkably low activation energy (0.32 eV). The extraordinarily high values of oxide ion conductivity reported for these phases are equivalent or better than the current state-of-the-art oxide ion conducting ceramics used in intermediate temperature solid oxide fuel cells, whilst leaving the possibility of further improvement *via* chemical and microstructural optimisation. It was proposed that oxygen vacancies were incorporated into these materials *via* an aliovalent doping strategy (eqn (1)) that substitutes Sr with alkali metals (Na or K) which is unusual as these are typically avoided as dopants, as previously discussed.[1]

$$Na_2O \xrightarrow{SrSiO_3} 2Na'_{Sr} + O^{\times}_O + V^{\cdot\cdot}_O \quad (1)$$
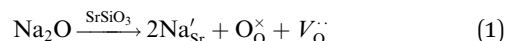
The structural chemistry, total conductivity and oxide ion conductivity of the nominally $Sr_{0.8}K_{0.2}Si_{0.5}Ge_{0.5}O_{2.9}$ phase, reported to have a conductivity of 1.04×10^{-2} S cm^{-1} at 625 °C, has been questioned.[1] During attempts to directly determine the oxygen ion diffusivity of the nominally $Sr_{0.8}K_{0.2}Si_{0.5}Ge_{0.5}O_{2.9}$ composition, Bayliss *et al.* have shown it to be a multi-phase material, with Rietveld analysis of neutron powder diffraction (NPD) data showing neither evidence for successful K doping on the Sr sites, nor a significant concentration of O vacancies, contrary to the previous report.[4] Furthermore, the work shows significantly lower levels of total conductivity than previously reported and no evidence of any significant oxide ion conductivity based on ^{18}O isotopic tracer diffusion measurements.

This journal is © The Royal Society of Chemistry 2014

J. Mater. Chem. A, 2014, **2**, 17919–17924 | 17919

In light of the new findings for the nominally $Sr_{0.8}K_{0.2}Si_{0.5}Ge_{0.5}O_{2.9}$ composition, in this work we reinvestigate the structural chemistry, microstructure and total conductivity of the highest conducting Na-doped phase reported to date, nominally $Sr_{0.55}Na_{0.45}SiO_{2.775}$. We attempt to rationalise our findings through a density functional theory computational approach with respect to the defect chemistry energetics.

Methods

Experimental

Samples of $Sr_{0.55}Na_{0.45}SiO_{2.775}$ were synthesised from $SrCO_3$ (Sigma-Aldrich >99.9%), Na_2CO_3 (Sigma-Aldrich >99.9999%) and SiO_2 (Sigma-Aldrich >99.9%). The samples were intimately ground together and heated according to the literature reports, with heating and cooling rates of 300 °C h^{-1}.[3] Pellets were prepared by uniaxial pressing of the powder with ~3 tons of pressure, followed by isostatic pressing at ~300 MPa before sintering. Samples for further analysis were polished sequentially to a ¼ micron roughness with diamond paste.

Neutron powder diffraction (NPD) data were obtained at ambient temperature on the GEM diffractometer at ISIS, Oxford, UK. The sample was loaded into an 8 mm diameter thin-walled cylindrical vanadium sample can and data collected at room temperature for 2 hours. The high resolution bank (backscattered detector 168°) was used for analysis in the structural work presented here. The program GSAS[7] was used for Rietveld structure refinements, in conjunction with the user interface EXPGUI for neutron diffraction data.[8]

Two-point AC impedance spectroscopy measurements were performed on pellets in dry and wet flowing air to examine the total conductivity (bulk and grain boundary) as a function of temperature using a Solartron 1260 frequency response analyser. Measurements were made in the frequency range of 1 Hz to 10 MHz with an AC amplitude of 10 mV. Platinum electrodes were painted onto the entire surface of the pellets and sintered at 900 °C for 1 hour. The sample was held in good contact with the Pt electrode mesh during the experiment by a spring mechanism. The total sample conductance for each temperature was determined by the intercept of the electrode arc with the real Z' axis (pellet diameter 12.8 mm, length 5.5 mm). Time-of-flight secondary ion mass spectrometry (IONTOF ToF-SIMS 5) was used to map the elemental composition of the samples using a 25 keV Bi^+ analytical ion beam with a 2 keV O_2^+ sputter beam to remove surface damage. A low energy electron flood gun (20 eV) was also applied for charge compensation. The SIMS instrument was operated under an analysis mode that facilitates a lateral resolution of approximately 200 nm.

Computational

All density functional theory (DFT) calculations were performed using the VASP code.[9,10] Interactions between the core and valence electrons are described within the projector augmented wave (PAW) method.[11] The calculations were performed using the Perdew Burke Ernzerhof (PBE) sol exchange–correlation functional, a revision of the successful PBE functional

specifically tailored for solids, which has been shown to yield structural data in excellent agreement with experiment.[12] A planewave cutoff of 750 eV and a k-point sampling of $2 \times 4 \times 2$ for the 60 atom unit cell of $SrSiO_3$ were used, with the ionic forces converged to less than 0.01 eV Å^{-1}. Defects were calculated in a $1 \times 2 \times 1$ (120) atom supercell with a $2 \times 2 \times 2$ Monkhorst–Pack special k-point grid, and all calculations were spin polarized. Thus an isolated substitutional defect represents a stoichiometry of $Sr_{0.96}X_{0.04}SiO_3$.

The formation energy of a defect with charge state q is given by

$$\Delta H_f(D, q) = (E^{D,q} - E^H) + \sum_i n_i(E_i + \mu_i)$$

where E^H is the total energy of the host supercell and $E^{D,q}$ is the total energy of the defect-containing cell. Elemental reference energies, E_i, were obtained from calculations on the constituent elements in their standard states, *i.e.*, $Sr_{(s)}$, $Si_{(s)}$, $K_{(s)}$, $Na_{(s)}$ and $O_{2(g)}$. μ_i is the chemical potential of the species in question, and n is the number of atoms added to or taken from an external reservoir.

Results and discussion

A Rietveld analysis was performed on energy-dispersive NPD data collected from a powder sample, with the initial model based on the data presented for the $Sr_{0.55}Na_{0.45}SiO_{2.775}$ composition from the literature.[3] Similarly to the K-doped phase, a reasonable fit could be achieved using this nominal composition model. However, on attempting to refine the Na to Sr ratio, significantly better statistical fits were achieved using models with no Na occupancy on the Sr site, suggesting there is little structural evidence for alkali metal doping in these phases. It is of further interest to note that no significant changes were apparent in the lattice cell parameters reported by Singh and Goodenough with increasing x in both $Sr_{1-x}K_xSi_{0.5}Ge_{0.5}O_{x-0.5x}$ or $Sr_{1-x}Na_xSiO_{3-0.5x}$ compositions, which may be expected if successful alkali metal doping on the Sr sites had indeed occurred.[2,3] The final structural refinement of the NPD data is presented in this work (Fig. 1) following refinement of the lattice cell parameters, atomic coordinates, site occupancies and isotropic displacement parameters (Table 1). It is interesting to note that small concentrations of vacancies (~3%) were found to be present on the O sites. We suspect this is likely to be due to minor Sr deficiency which was also present in the refinement. Further investigations into the Na doped and Sr deficient phases will be published elsewhere.[13,14]

Total conductivity has been investigated (bulk and grain boundary) using AC impedance spectroscopy. All impedance spectra obtained consisted of single, depressed arcs and were fitted to a single resistor and constant phase element in parallel. The arc is significantly depressed indicating a distribution of relaxation times which is consistent with the inhomogeneity of the sample microstructure, demonstrated later in this work. Example impedance spectra are shown in Fig. S1 in the ESI† in both dry and wet conditions.
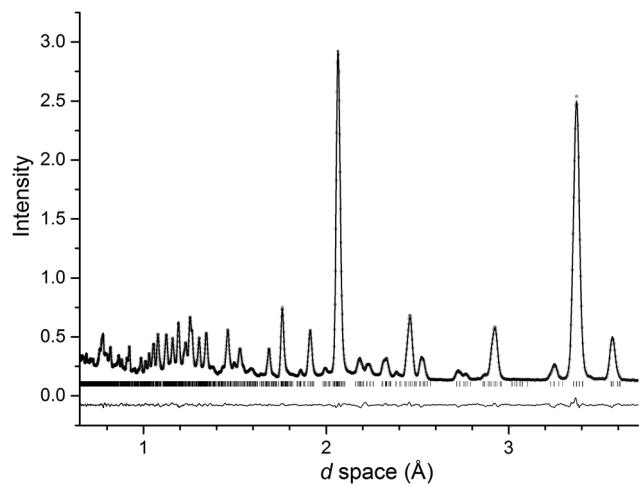
17920 | *J. Mater. Chem. A*, 2014, **2**, 17919–17924

This journal is © The Royal Society of Chemistry 2014

Fig. 1 Final Rietveld fit of ambient temperature time-of-flight neutron powder diffraction data showing observed data (●), calculated and difference profiles (continuous lines), and reflection positions (|). Goodness-of-fit values of $R_{wp} = 0.021$, $R_p = 0.018$, $\chi^2 = 3.69$ reflect the excellent agreement between the model and data.

Table 1 Final structural parameters for $SrSiO_3$ obtained from the nominally $Sr_{0.55}Na_{0.45}SiO_{2.775}$ composition of interest from ambient temperature time-of-flight NPD data showing final atomic coordinates, site occupancy and isotropic atomic displacements. Space group $C2/c$. $a = 12.3417(8)$ Å, $b = 7.1463(4)$ Å, $c = 10.8922(5)$ Å, $\beta = 111.623(3)°$

Element	x	y	z	Fraction	$U_i/U_e \times 100$
Sr 1	0.0864(3)	0.2434(4)	0.4997(5)	0.96(1)	0.4(1)
Sr 2	0.25	0.25	0	1	1.0(2)
Si 1	0.1244(6)	0.4573(9)	0.2461(5)	1	0.2(1)
Si 2	0	0.833(2)	0.25	1	3.1(3)
O 1	0.1261(4)	0.4082(9)	0.1063(4)	0.98(1)	1.0(1)
O 2	0.2220(3)	0.4091(9)	0.3870(3)	1	0.7(1)
O 3	0.1069(4)	0.6874(6)	0.2496(4)	0.93(1)	0.2(1)
O 4	0.0480(3)	0.9351(9)	0.3898(3)	1	0.8(1)
O 5	0	0.366(1)	0.25	0.93(2)	0.6(3)

The conductivities determined from the extracted resistance and sample dimensions are plotted along with literature data for the equivalent composition in Fig. 2. The data recorded in this work was performed in both dry flowing air and in air bubbled through water held at 50 °C, showing identical conductivities in both atmospheres. The results show, similarly to those observed for the K doped phases, substantially reduced total conductivity compared to the previously reported literature values. The total conductivity observed in this work is typically at least an order of magnitude lower than previously reported. The sample was also held at approximately 580 °C in flowing humid air and the total conductivity was found to linearly decrease over the duration of 20 hours, by which point the conductivity had dropped by approximately half an order of magnitude. These data points are labelled A in Fig. 2. The conductivity results measured in humid atmospheres suggest that protons are not responsible for the high conductivity
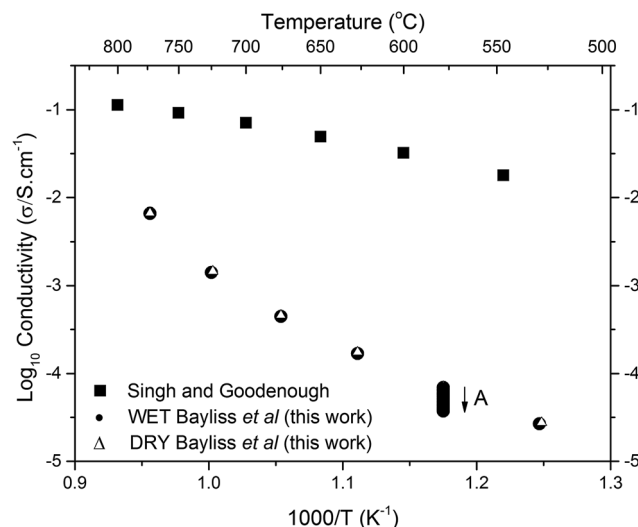

Fig. 2 Arrhenius plot of total conductivity from literature values and those from this work in both dry and wet atmospheres as a function of reciprocal temperature. The figure highlights difference in total conductivity between the work reported in the literature[3] and recorded during this work. The arrow labelled A shows the wet sample held at a temperature for 20 hours and measurements every hour, showing increasing samples resistance.

previously proposed in these materials. Similarly to the K doped samples, upon holding in a humid atmosphere, the Na doped samples were observed to physically degrade, suggesting a potential source for the increased resistance. The variable $p(O_2)$ measurements reported by Wei et al.[5] are the only evidence put forward for the oxide ionic nature of the conduction mechanism, however the $p(O_2)$ independence of total conductivity is only able to show that the concentration of the dominant charge carrier is $p(O_2)$ independent, which would be the case for other conduction mechanisms including extrinsic Na ion conduction.

While impressive fuel cell measurements have been reported for the nominally $Sr_{0.55}Na_{0.45}SiO_{2.775}$ composition, our results both here and for the K doped materials[1] suggest that it is not related to oxide ion or proton conductivity. While the fuel cell measurements do prove that the material is not electronically conducting, it does not preclude other electrochemical processes taking place. Wei et al. report an abnormally high open circuit voltage (OCV) of ~1.24 V at between 500–650 °C, whilst the Nernst equation would predict lower maximum values.[15] One way this high value could be explained is through the minimal production of water at the anode due to a lack of oxygen ion carriers, making the reaction quotient value in the Nernst equation very low.

In a similar manner to our previous publication,[1] ToF-SIMS ion mapping has been performed to study the elemental distribution of cut and polished sections of a pellet. Fig. 3 shows a multiphase composition with elemental mapping indicating oxide phases composed of Sr- and Si-, Na- and Si- and Si-rich regions, analogous to the nominally $Sr_{0.8}K_{0.2}Si_{0.5}Ge_{0.5}O_{2.9}$ composition.[1] The multiple phase composition and lack of evidence for secondary crystalline phases in the diffraction data
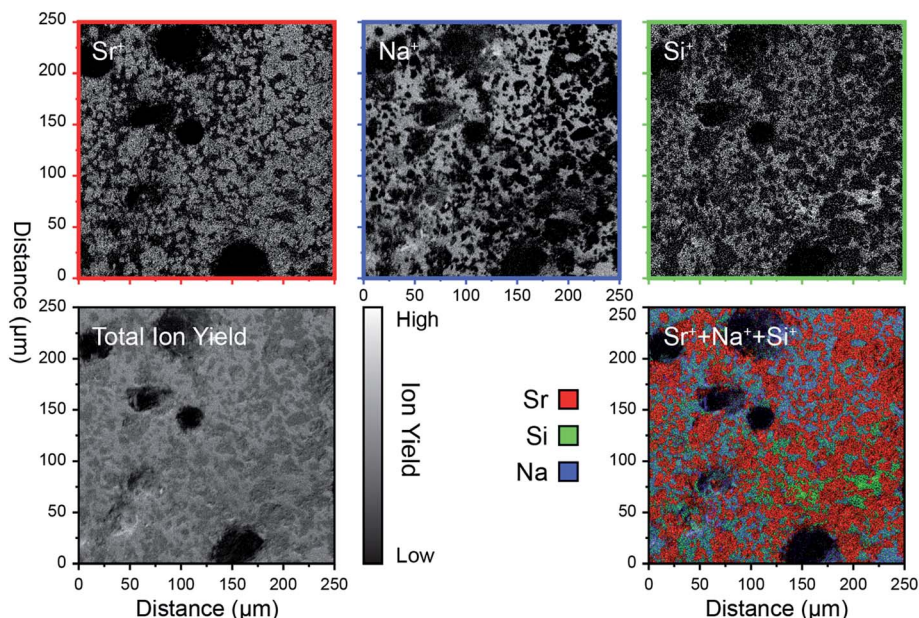
Fig. 3 ToF-SIMS chemical ion mapping over an area of 250 × 250 μm^2, clearly showing an inhomogeneous elemental distribution, leading to the conclusion that these materials are not single phase.

suggest that the Na–Si and Si type oxides are amorphous, however, it is not possible to directly determine from this data. We propose the amorphous phase is likely to be a Na$_2$SiO$_3$-type material, discussed in more detail previously, though further investigation is required to confirm its exact composition.[1]

In order to investigate the thermodynamics of alkali metal solubility in SrSiO$_3$ as an acceptor dopant, density functional theory calculations have been performed. By varying the chemical potentials, μ_i, we can simulate the effect of varying the partial pressures experimentally, setting the conditions under which SrSiO$_3$ forms. In this way, we can determine the optimum conditions for defect formation, within the constraint of the calculated enthalpy of the host:

$$\mu_{Sr} + \mu_{Si} + 3\mu_O = \Delta H_f^{SrSiO_3}$$

To avoid precipitation into solid elemental Sr, Si, and gaseous O$_2$ we also require:

$$\mu_{Sr} \leq 0 \text{ eV}; \; \mu_{Si} \leq 0 \text{ eV}; \; \mu_O \leq 0 \text{ eV}$$

The chemical potentials are further constrained by the decomposition of SrSiO$_3$ into competing binary and ternary compounds. For SrSiO$_3$, we find that the major limiting phases are the binary SiO$_2$ (alpha quartz) ($\mu_{Si} + 2\mu_O = \Delta H_f^{(SiO_2)}$) and the ternary phase Sr$_2$SiO$_4$ ($2\mu_{Sr} + \mu_{Si} + 4\mu_O = \Delta H_f^{Sr_2SiO_4}$). This is consistent with the PBE screening from the Materials Project,[16] although this also found that Si$_6$O$_{13}$ slightly cuts into the stability field of SrSiO$_3$, which does not occur using our PBEsol method. It should be noted that the PBEsol method is a revision of the PBE method, designed specifically for modelling solids.
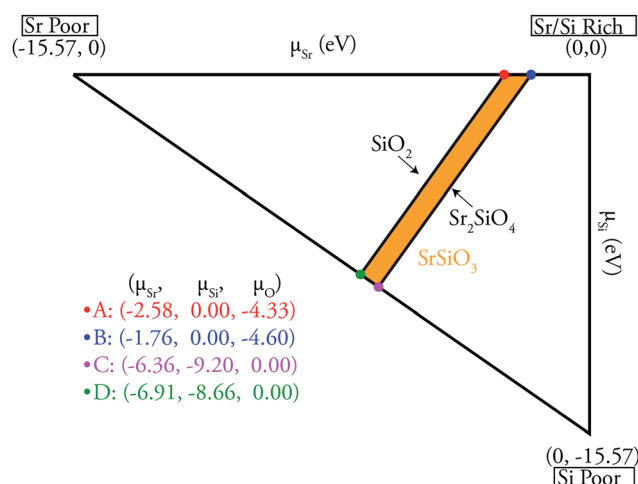

Fig. 4 Illustration of the accessible (μ_{Sr}, μ_{Si}) chemical potential range. The triangle vertices are determined by the formation enthalpy of SrSiO$_3$. Limits imposed by the formation of competing binary and ternary oxides result in the stable region shaded orange. Environments A, B, C, D are indicated by the red, blue, pink and green spheres respectively. All chemical potentials are given in eV.

The PBEsol calculated accessible range of chemical potentials for SrSiO$_3$ is illustrated in Fig. 4 in a two-dimensional (μ_{Sr}, μ_{Si}) plane, following the standard approach,[17,18] and generated using the CPLAP code.[19] The vertices of the stability triangle are formed from the host conditions ($\mu_{Sr} + \mu_{Si} + 3\mu_O \leq \Delta H_f^{SrSiO_3}$), giving the limits of Sr/Si rich, Sr-poor and Si-poor environments. Taking into account the constraints imposed by the competing phases, the stable range of (μ_{Sr}, μ_{Si}) for SrSiO$_3$ is shaded orange in Fig. 4. Within these boundaries, we explicitly considered four environments, (A, B, C and D) as indicated on Fig. 4. A and B

17922 | *J. Mater. Chem. A*, 2014, **2**, 17919–17924

This journal is © The Royal Society of Chemistry 2014

correspond to Si-rich, Sr-rich and O-poor conditions, and are expected to be optimum for n-type defect formation, whereas C and D represents the Sr-poor/Si-poor/O-rich limit and is expected to favour the formation of p-type defects.

For each of the four representative limits, we have calculated the formation energy of the native point defects, with the results displayed in Table 2. In the SrSiO$_3$ crystal structure there are two distinct Sr sites, two Si sites and 5 oxygen sites, as indicated in Fig. 5.

It is clear that under conditions A and B (oxygen poor), the oxygen vacancy ($V_O^{\cdot\cdot}$) is the dominant intrinsic defect, as is expected. Under conditions C and D, the formation of an O_i'' is favoured over the formation of a V_{Sr}'' or V_{Si}''''. Experimentally, samples are more likely to be grown in conditions closer to

conditions C and D, where oxygen excess, or strontium deficient samples are to be expected.

When considering the doping of K or Na into the system, we can determine the likelihood of this occurrence using the relationship:

$$M_2O_{(s)} + Sr_{24}Si_{24}O_{72(s)} \rightarrow Sr_{22}M_2Si_{24}O_{71(s)} + 2SrO_{(s)}$$
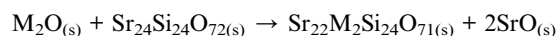
i.e.

$$\Delta H^f = [E(Sr_{22}M_2Si_{24}O_{71(s)}) + 2 \times E(SrO_{(s)})] - [E(M_2O_{(s)}) + E(Sr_{24}Si_{24}O_{72(s)})]$$

where M = K or Na and $E(X)$ is the energy of the species of interest obtained directly from the VASP calculations. To test this, we have calculated the ΔH^f of 5 complexes involving either K or Na on two Sr sites neighbouring each of the distinct oxygen sites. The formation energies of these complexes are shown in Table 3. It is immediately clear from the large formation energies that a solid solution between M$_2$O and SrSiO$_3$ is not expected to form, and large concentrations of K and Na are not expected to be present in SrSiO$_3$.

In addition, we can calculate the association energy (or interaction energy) of the complex from the formula,

$$\Delta H_{Association} = \Delta H_{Separated} - \Delta H_{Complex}$$

which is defined as the difference between the formation energy of the complex and the individual formation energies of the non-interacting, isolated defects that make up the complex. The calculated association energies for both K and Na based clusters are presented in Table 3. These large association energies indicate that there is a very large driving force for the charge compensating vacancy to be situated next to the acceptor dopants, trapping the vacancy near the dopants and increasing the barrier to effective oxide ion vacancy transport. To summarise, even if these high energy defects formed, we calculate that the vacancy would be strongly trapped and thus would not be expected to contribute high oxide ion conductivity which is not consistent with the low activation energy of 0.32 eV measured.[5]

Table 2 Formation energy of all defects (in eV) considered in SrSiO$_3$ in the neutral charge state at the 4 chemical potential limits from Fig. 5

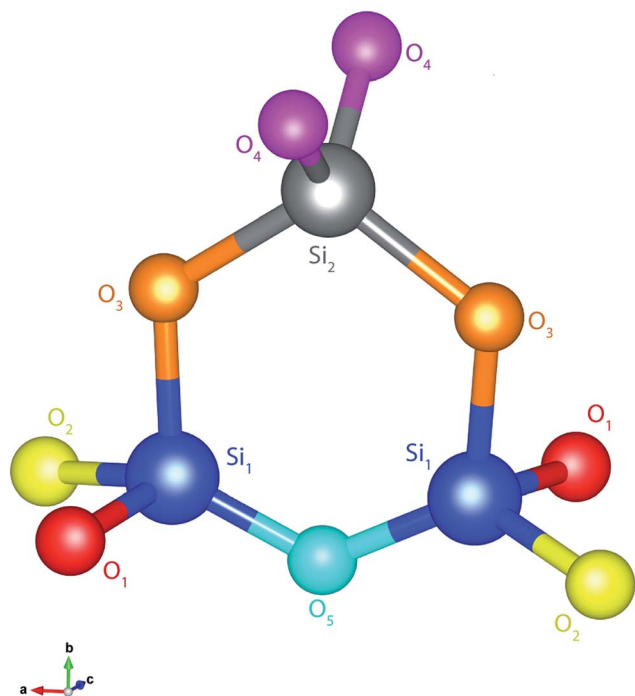| Defect	A (eV)	B (eV)	C (eV)	D (eV)
$V_{O1}^{\cdot\cdot}$	1.18	0.91	5.51	5.51
$V_{O2}^{\cdot\cdot}$	1.17	0.89	5.50	5.50
$V_{O3}^{\cdot\cdot}$	1.13	0.86	5.47	5.47
$V_{O4}^{\cdot\cdot}$	1.16	0.89	5.49	5.49
$V_{O5}^{\cdot\cdot}$	1.17	0.90	5.50	5.50
V_{Sr1}''	8.22	9.04	4.16	3.89
V_{Sr2}''	8.18	8.99	4.12	3.85
V_{Si1}''''	15.93	15.93	6.73	7.27
V_{Si2}''''	15.94	15.94	6.74	7.28
O_i''	6.93	7.20	2.60	2.60

Fig. 5 Illustration of the structure around a Si$_3$O$_9$ secondary building unit, indicating the 2 crystallographically distinct Si environments and the 5 distinct oxygen environments.

Table 3 Formation energy of K and Na complexes with compensating oxygen vacancies in SrSiO$_3$. The second column holds the $\Delta H_{Association}$ for each complex. All energies are given in eV

Defect	ΔH^f (eV)	$\Delta H_{Association}$ (eV)
$2K_{Sr}' + V_{O1}^{\cdot\cdot}$	4.13	3.86
$2K_{Sr}' + V_{O2}^{\cdot\cdot}$	4.24	3.74
$2K_{Sr}' + V_{O3}^{\cdot\cdot}$	4.95	3.00
$2K_{Sr}' + V_{O4}^{\cdot\cdot}$	4.16	3.80
$2K_{Sr}' + V_{O5}^{\cdot\cdot}$	5.03	2.99
$2Na_{Sr}' + V_{O1}^{\cdot\cdot}$	4.88	3.91
$2Na_{Sr}' + V_{O2}^{\cdot\cdot}$	4.89	3.89
$2Na_{Sr}' + V_{O3}^{\cdot\cdot}$	5.86	2.89
$2Na_{Sr}' + V_{O4}^{\cdot\cdot}$	4.92	3.85
$2Na_{Sr}' + V_{O5}^{\cdot\cdot}$	5.76	3.07

Table 4 Calculated effects of the defect formation on the modelled lattice constant for the concentrations considered in this study

System	V (Å^3)	ΔV (Å^3)	%ΔV	a (Å)	b (Å)	c (Å)
Pure supercell	1783.250	0.000	0.000	12.336	7.145	10.882
$2K'_{Sr} + V_{O1}^{\cdot\cdot}$	1799.540	16.290	0.914	12.449	7.211	10.982
$2Na'_{Sr} + V_{O1}^{\cdot\cdot}$	1785.570	2.320	0.130	12.352	7.155	10.897
K'_{Sr1}	1787.320	4.070	0.228	12.364	7.162	10.907
Na'_{Sr1}	1779.110	−4.140	−0.232	12.308	7.129	10.857
$V_{O1}^{\cdot\cdot}$	1777.150	−6.100	−0.342	12.294	7.121	10.845

We have also calculated the effect of the defect formation on the lattice constant for the concentrations considered in this study, with the results presented in Table 4. The formation of $V_O^{\cdot\cdot}$ and Na'_{Sr} cause compression of the unit cell, while K'_{Sr} causes an expansion of the lattice, as is expected on ionic radii grounds. Complex formation causes a larger expansion of the lattice than the simple sum of the relaxations of the constituent elements. In fact, for the Na complex, the overall effect is a lattice expansion, even though the individual defects making up the complex display lattice contractions. This is in contrast with the lack of lattice cell parameter change present in the previous purportedly single phase materials.[2–4]

Conclusions

In this work we have demonstrated that the Na doped SrSiO$_3$ type oxide is not single phase, analogous to the nominally K-doped Sr(Si,Ge)O$_3$ system previously reported by the authors. We have demonstrated that samples prepared with the synthetic conditions originally reported show multiphase composition by ToF-SIMS ion mapping, no evidence for Na substitution in the crystalline SrSiO$_3$ phase by Rietveld refinement of NPD data, and significantly lower total conductivity than previously reported.

A density functional theory computational study has concluded that the formation of native defects in the SrSiO$_3$ phase is not only energetically unfavourable, but moreover should these defects exist, their mobility would be limited due to the formation of strong defect associations. Finally, lattice relaxation calculations suggest that unit cell changes would be expected on doping, in contrast to the original experimental studies.

Acknowledgements

References

1 R. D. Bayliss, S. N. Cook, S. Fearn, J. A. Kilner, C. Greaves and S. J. Skinner, *Energy Environ. Sci.*, 2014, DOI: 10.1039/c4ee00734d.

2 P. Singh and J. B. Goodenough, *Energy Environ. Sci.*, 2012, **5**, 9626.

3 P. Singh and J. B. Goodenough, *J. Am. Chem. Soc.*, 2013, **135**, 10149.

4 R. Martinez-Coronado, P. Singh, J. Alonso-Alonso, J. B. Goodenough, R. Martinez and J. A. Alonso, *J. Mater. Chem. A*, 2014, **2**, 4355.

5 T. Wei, P. Singh, Y. Gong, J. B. Goodenough, Y. Huang and K. Huang, *Energy Environ. Sci.*, 2014, **7**, 1680.

6 J. Xu, X. Wang, H. Fu, C. M. Brown, X. Jing, F. Liao, F. Lu, X. Li, X. Kuang and M. Wu, *Inorg. Chem.*, 2014, **53**, 6962.

7 A. C. Larson and R. B. Von Dreele, *General Structure Analysis System (GSAS)*, *Los Alamos National Laboratory Report LAUR 86-748*, Los Alamos, 2004, 86–748.

8 B. H. Toby, *J. Appl. Crystallogr.*, 2001, **34**, 210.

9 G. Kresse and J. Hafner, *Phys. Rev. B: Condens. Matter Mater. Phys.*, 1994, **49**, 14251.

10 G. Kresse and J. Furthmüller, *Phys. Rev. B: Condens. Matter Mater. Phys.*, 1996, **54**, 11169.

11 G. Kresse and D. Joubert, *Phys. Rev. B: Condens. Matter Mater. Phys.*, 1999, **59**, 11.

12 J. Perdew, A. Ruzsinszky, G. Csonka, O. Vydrov, G. Scuseria, L. Constantin, X. Zhou and K. Burke, *Phys. Rev. Lett.*, 2008, **100**, 136406.

13 P. Keenan, O. Cross, J. M. Porras-Vazquez and P. R. Slater, 2014, manuscript in preparation.

14 I. R. Evans, J. S. O. Evans, H. G. Davies, A. R. Haworth and M. L. Tate, *Chem. Mater.*, 2014, DOI: 10.1021/cm502850m.

15 W. Nernst, *Z. Phys. Chem.*, 1889, **4**, 29.

16 A. Jain, S. P. Ong, G. Hautier, W. Chen, W. D. Richards, S. Dacek, S. Cholia, D. Gunter, D. Skinner, G. Ceder and K. A. Persson, *APL Mater.*, 2013, **1**, 011002.

17 D. O. Scanlon, *Phys. Rev. B: Condens. Matter Mater. Phys.*, 2013, **87**, 161201.

18 D. O. Scanlon, P. D. C. King, R. P. Singh, A. de la Torre, S. M. Walker, G. Balakrishnan, F. Baumberger and C. R. A. Catlow, *Adv. Mater.*, 2012, **24**, 2154.

19 J. Buckeridge, D. O. Scanlon, A. Walsh and C. R. A. Catlow, *Comput. Phys. Commun.*, 2014, **185**, 330.